

Quantification of global orientational order in organic solids by magic-angle spinning deuterium NMR with rotor synchronization

Magesh Nandagopal

Institute of Materials Science, University of Connecticut, Storrs, Connecticut 06269

Marcel Utz^{a)}

*Institute of Materials Science, University of Connecticut, Storrs, Connecticut 06269
and Department of Physics, University of Connecticut, Storrs, Connecticut 06269*

(Received 8 July 2005; accepted 11 October 2005; published online 23 December 2005)

A new method for the characterization of orientational order in organic solids based on magic-angle spinning NMR spectroscopy is introduced. The method is related to the rotor-synchronized magic-angle spinning experiment proposed by Harbison and Spiess [Chem. Phys. Lett. **124**, 128 (1986)], but exploits the anisotropy of the deuterium quadrupolar coupling instead of the carbon-13 chemical shielding anisotropy. Magic-angle spinning provides a sensitivity advantage over pseudostatic techniques; using the deuterium quadrupolar coupling makes the method applicable to systems that do not exhibit large carbon chemical shift anisotropies, such as aliphatic polymers. Due to the magnitude of the deuterium quadrupolar coupling, a large number of spinning sidebands can be reliably observed, allowing for a precise determination of the orientational distribution function. Experimental data are analyzed in terms of Wigner matrix basis functions as well as the conjugate orthogonal functions framework. Unidirectionally cold-drawn poly(ethylene) is used as an example to demonstrate the method. © 2005 American Institute of Physics. [DOI: [10.1063/1.2132274](https://doi.org/10.1063/1.2132274)]

I. INTRODUCTION

Many organic solids are globally anisotropic, and their physical properties can strongly depend on the nonuniform distribution of molecular orientation. Examples include polymers processed by extrusion, film blowing, cold drawing, or fiber spinning, but also biological structural materials, such as spider silk, chitin, cellulose, and collagen. In principle, many macroscopic probes are sensitive to the molecular order, such as optical birefringence, or mechanical (elastic) anisotropy. However, measuring these quantities only provides an overall indication of the orientational order. In order to obtain a molecularly resolved picture of the structural order, it is necessary to resort to spectroscopic techniques which provide molecular specificity. The most important practical alternatives are infrared spectroscopy, which provides orientational information through linear dichroism, and NMR spectroscopy.

Quantification of orientational order by NMR is based on terms in the nuclear-spin Hamiltonian which depend on the orientation of the relevant interaction tensor with respect to the imposed static magnetic field. The observable transition frequency for each molecular segment depends on its orientation with respect to the magnetic field. The resulting inhomogeneously broadened NMR line shape therefore contains information on the distribution of molecular orientations in the sample. Various methods based on this common principle have been described, using the chemical shielding anisotropy¹⁻¹⁰ and the quadrupolar interaction,¹¹ as well as the anisotropic dipolar coupling.¹²

Due to the uniaxial symmetry of the external magnetic field, NMR experiments are invariant under a rotation of the sample around the z axis. Without further precautions, only a correspondingly averaged molecular orientational distribution function can therefore be determined from NMR spectra. This limitation can be overcome by taking into account one-dimensional spectra at different orientations of the sample with respect to a rotation about a horizontal axis.⁹ More elegantly, two different orientations can be correlated in a two-dimensional experiment.^{6,7,11} This direction exchange with correlation for orientation-distribution evaluation and reconstruction (DECODER) method produces a two-dimensional intensity pattern, which reflects the full orientational distribution function of the molecular segment under study.

Another route to breaking this symmetry is taken by the rotor-synchronized (r-sync) magic-angle spinning (MAS) experiment.^{4,5} This is a two-dimensional experiment in which the rotor phase is incremented from 0 to 2π in the indirect dimension. Fourier transformation yields a two-dimensional manifold of sideband intensities which reflect the orientational order in the sample. This approach is attractive, since it conserves the sensitivity advantage of MAS NMR. To our knowledge, this principle has only been used in conjunction with the ¹³C chemical shielding anisotropy up to now. This works very well for systems that contain carbon atoms with large chemical shift anisotropies (CSAs), such as phenylene rings and carbonyl groups. However, even in favorable cases, the number of sidebands that is available for analysis is highly limited. ¹³C chemical shielding anisotropies are rarely substantially more than 100 ppm. Particularly in amorphous solids, where there is considerable spread of

^{a)}Electronic mail: marcel.utz@uconn.edu; URL: <http://giotto.ims.uconn.edu/~mutz>

the isotropic part of the chemical shift, only five to ten sidebands can usually be resolved. This limits the amount of orientational information that can be obtained. In many cases of interest, the ^{13}C chemical shielding anisotropies are much less than 100 ppm, for example, in aliphatic polymers such as poly(ethylene), poly(propylene), and in polyethers such as poly(oxy methylene) and poly(ethylene oxide). In these materials, deuteration provides an attractive alternative.

This contribution demonstrates the use of the rotor-synchronized MAS method with the quadrupolar coupling of ^2D nuclei, thus extending the applicability of the r-sync MAS method to organic solids with small CSA tensors, such as aliphatic polymers. The ^2D quadrupolar coupling in organic solids is typically of the order of 170 kHz, as opposed to the CSAs, which are below 20 kHz even in favorable cases and at large field strengths. At the same time, the isotropic chemical shifts are much smaller in the case of ^2D than ^{13}C . Particularly in the case of glassy systems, this leads to a substantially larger number of observable sidebands in the magic-angle spinning spectrum, which can be exploited to obtain orientational information using the rotor-synchronized MAS method. An important advantage of ^2D NMR is the well-defined orientation dependence of the quadrupolar interaction, which is uniaxial with its axis along the C– ^2H bond, within 3° .⁸ A slight drawback is that this direction is not along the chain axis, which is usually the direction of interest.

The r-sync MAS approach offers, over the quasistatic DECODER experiment, the advantage of substantially greater sensitivity, since the spectral intensity is concentrated into discrete sidebands. Of course, the higher the MAS frequency, the larger the S/N ratio. At the same time, however, information on the molecular orientation is lost due to the diminishing number of observable sidebands. As detailed below, the r-sync MAS approach allows for a balanced compromise between signal/noise and orientational sensitivity by a careful choice of the magic-angle spinning speed.

The advantages of ^2D spectroscopy—spectroscopic and orientational sensitivity, ease of data interpretation—come at a price. In the case of ^{13}C , it is often possible to work with natural abundance, whereas ^2D spectroscopy always necessitates isotopic labeling. The isotropic chemical shift of ^{13}C allows for the simultaneous observation of several MAS sideband manifolds in samples that have several sites. Similar molecular specificity is only offered by ^2D if selective labeling is used.

II. THEORETICAL BACKGROUND

The Hamiltonian governing the evolution of a ^2D nucleus is given by

$$\mathcal{H}_q = -\gamma B_0(1 - \sigma)I_z + N_Q \frac{\sqrt{6}}{6} V_{2,0} (3I_z^2 - I(I+1)), \quad (1)$$

where γ is the gyromagnetic ratio, B_0 the external magnetic field, σ the chemical shift, $V_{2,0}$ denotes a spherical component of the electric-field gradient tensor, and N_Q is the quadrupolar coupling constant,

$$N_Q = \frac{eQ}{2I(2I-1)\hbar}, \quad (2)$$

with the nuclear quadrupole moment Q . Both the chemical shift σ and the relevant component of the electric-field gradient (EFG) $V_{2,0}$ depend on the orientation of the molecular frame with respect to the magnetic field \mathbf{B}_0 . In the case of ^2D , the chemical shifts are very small (of the order of a few ppm, corresponding to a few hundred hertz at typical field strengths), and can be neglected in comparison to the quadrupolar coupling, which is of the order of 100 kHz. The same applies to scalar couplings between ^2D nuclei. However, dipolar couplings between nearest-neighbor deuterons can be significant, and would in principle have to be included in the discussion. In the present case, however, we are using magic-angle spinning speeds around 10 kHz, which are large enough to eliminate these terms; the dipolar coupling constant between geminal ^2D in a methylene group is around 2 kHz.

The quadrupolar coupling is proportional to the laboratory-frame zz component of the EFG tensor at the location of the ^2D nucleus, and therefore transforms as a second-rank spherical tensor. The EFG \mathbf{V} can be expressed as a spherical tensor with the components

$$V_{2,0}^{\text{PAS}} = \frac{3}{\sqrt{6}}\delta, \quad V_{2,\pm 2}^{\text{PAS}} = \frac{1}{2}\delta\eta \quad (3)$$

in its principle-axis system (PAS), with $\delta = V_{zz}^{\text{PAS}}$ and $\eta \in [0, 1]$.

The strength of the quadrupolar interaction is often expressed in terms of the quadrupolar coupling constant,

$$C_Q = \frac{eQ\delta}{h}. \quad (4)$$

In the case of ^2D in a C–D bond, $C_Q \approx 170$ kHz.⁸

The interaction of the quadrupolar nuclei with the electric-field gradient tensor dictates the resulting line shape of the spectrum, which is characterized by the asymmetry η and the anisotropy δ . The asymmetry parameter of the electric-field gradient tensor associated with the aliphatic C– ^2H bond is negligible ($\eta=0$) due to the uniaxial charge distribution along the internuclear vector. The cylindrical symmetry also causes the z axis of the PAS of the electric-field gradient tensor to align with the C– ^2H internuclear vector to within 3° .⁸

Under magic-angle spinning, the orientational dependence of the Hamiltonian leads to a modulation of the spin evolution frequency, which becomes a periodic function of time. Herzfeld and Berger¹³ have given a seminal treatment of the resulting spinning sideband pattern for the closely related case of the chemical shift tensor. Their derivation is easily adapted to the quadrupolar interaction. The fact that $\eta=0$ leads to a significant simplification, since it is sufficient to indicate the orientation of the unique axis of the EFG in the sample frame, which can be done using only two Euler angles, instead of the three that are needed in the general case.

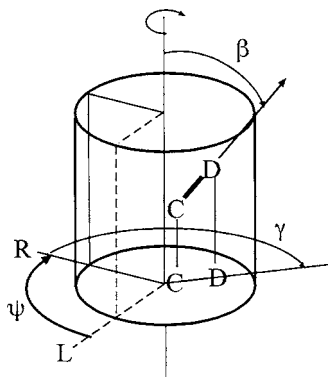


FIG. 1. Definition of polar angles γ and β , which orient the unique axis of the deuterium electric-field gradient tensor in the rotor frame, and the rotor reference phase angle ψ , which indicates the angle between the rotor orientation at the start of the NMR acquisition with respect to the laboratory reference frame.

The unique axis of the deuterium electric-field gradient tensor is related to the rotor frame by two Euler angles (γ and β). ψ is the rotor reference phase that relates the position of the rotor to the laboratory frame (Fig. 1).

Since $I=1$ for ^2D , each molecular orientation gives rise to two different transition frequencies, separated from the Zeeman frequency by equal amounts in opposite directions. From a theoretical viewpoint, this leads to two sideband manifolds, which superimpose to yield the observed spectrum. For a particular molecular segment oriented at (β, γ) , the intensities of the N th sideband in the two manifolds I_N^+ and I_N^- are

$$I_N^\pm = \frac{1}{2\pi} e^{iN\gamma} F(\pm\gamma) \int_0^{2\pi} e^{iN\vartheta} F(\pm\vartheta) d\vartheta, \quad (5)$$

where trivial constant prefactors have been omitted. The function $F(\vartheta)$ describes the variation of the resonance frequency during a MAS cycle, and is given by

$$F(\vartheta) = \exp(-i(\bar{A}_2 \sin 2\vartheta + \bar{A}_1 \sin \vartheta)), \quad (6)$$

with the constants

$$\bar{A}_1 = -\frac{3\sqrt{2}C_Q}{4\nu_r} \sin\beta \cos\beta, \quad (7)$$

and

$$\bar{A}_2 = \frac{3}{16} \frac{C_Q}{\nu_r} \sin^2\beta, \quad (8)$$

where ν_r denotes the magic-angle spinning frequency. Note that the constants \bar{A}_1 and \bar{A}_2 only depend on the angle β , which denotes the angle between the unique axis of the symmetric EFG tensor and the spinning axis. A nonvanishing asymmetry would introduce a dependence on the first Euler angle, considerably complicating the treatment.

The above expressions assume that the free induction decay is acquired in synchronization with the sample rotation, i.e., the sample reference direction (R in Fig. 1) is lined up with the laboratory reference direction (L in Fig. 1) at the instant of the excitation rf pulse. If this is not the case, the angle γ in the above equations is replaced by an angle

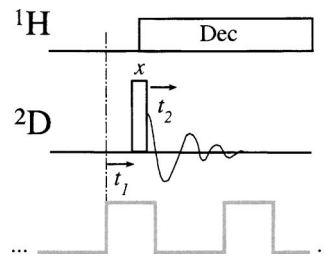


FIG. 2. Pulse sequence used for the rotor-synchronized MAS experiment. The acquisition is synchronized to the positive flank of the rotation speed detection signal.

$\gamma + \psi$, where ψ denotes the orientation offset of the sample at the beginning of the acquisition. As can be seen in Eq. (5), this leads to a nontrivial phase factor in the sideband intensities. This dependence on the starting phase of the rotor lies at the heart of the rotor-synchronized MAS technique.^{4,5}

As a short aside, the form of Eq. (5) makes it very easy to compute the spectrum resulting from an isotropic sample ("powder spectrum"). This requires averaging over all possible angles β and γ . The integration over γ yields

$$\bar{I}_N^-(\beta) = \frac{1}{4\pi^2} \int_0^{2\pi} d\gamma e^{iN\gamma} F(\pm\gamma) \int_0^{2\pi} d\vartheta e^{iN\vartheta} F(\pm\vartheta), \quad (9)$$

and likewise for \bar{I}_N^+ . The integration over the polar angle γ can therefore be expressed with the Fourier components of the function $F(\vartheta)$ as

$$\bar{I}_N^\pm(\beta) = \hat{F}_{\mp N} \hat{F}_{\mp N}, \quad (10)$$

where

$$\hat{F}_N = \frac{1}{2\pi} \int_0^{2\pi} e^{-iN\vartheta} F(\vartheta) d\vartheta. \quad (11)$$

A true powder average can therefore be computed very effectively using the fast Fourier transform algorithm. Note that $\bar{I}_N^+ = (\bar{I}_N^-)^*$. Therefore, the sum of the two contributions, which corresponds to the observable spectrum, is purely absorptive. Dispersive components only occur for samples with a nonuniform distribution of polar angles γ .

In order to quantify the distribution of orientations (β, γ) in the sample, the rotor-synchronized pulse sequence shown in Fig. 2 is used. In this case, the acquisition is started in sync with the sample rotation, with a time delay t_1 , which is incremented in equal steps from zero to the equivalent of an entire rotor period. This, in effect, increases the rotor phase angle ψ (Fig. 1). Subsequent Fourier transformation therefore yields a two-dimensional manifold of sidebands $I_{M,N} = I_{M,N}^+ + I_{M,N}^-$ with

$$I_{M,N}^\pm(\beta, \gamma) = \frac{e^{iN\gamma}}{4\pi^2} \int_0^{2\pi} e^{i(N-M)\psi} F(\pm(\gamma + \psi)) d\psi \times \int_0^{2\pi} e^{iN\vartheta} F(\pm\vartheta) d\vartheta. \quad (12)$$

The distribution of intensities $I_{N,M} = I_{N,M}^+ + I_{N,M}^-$ depends sensitively on the orientation of the molecular segment (β, γ) . Averaged over a disordered sample, the resulting

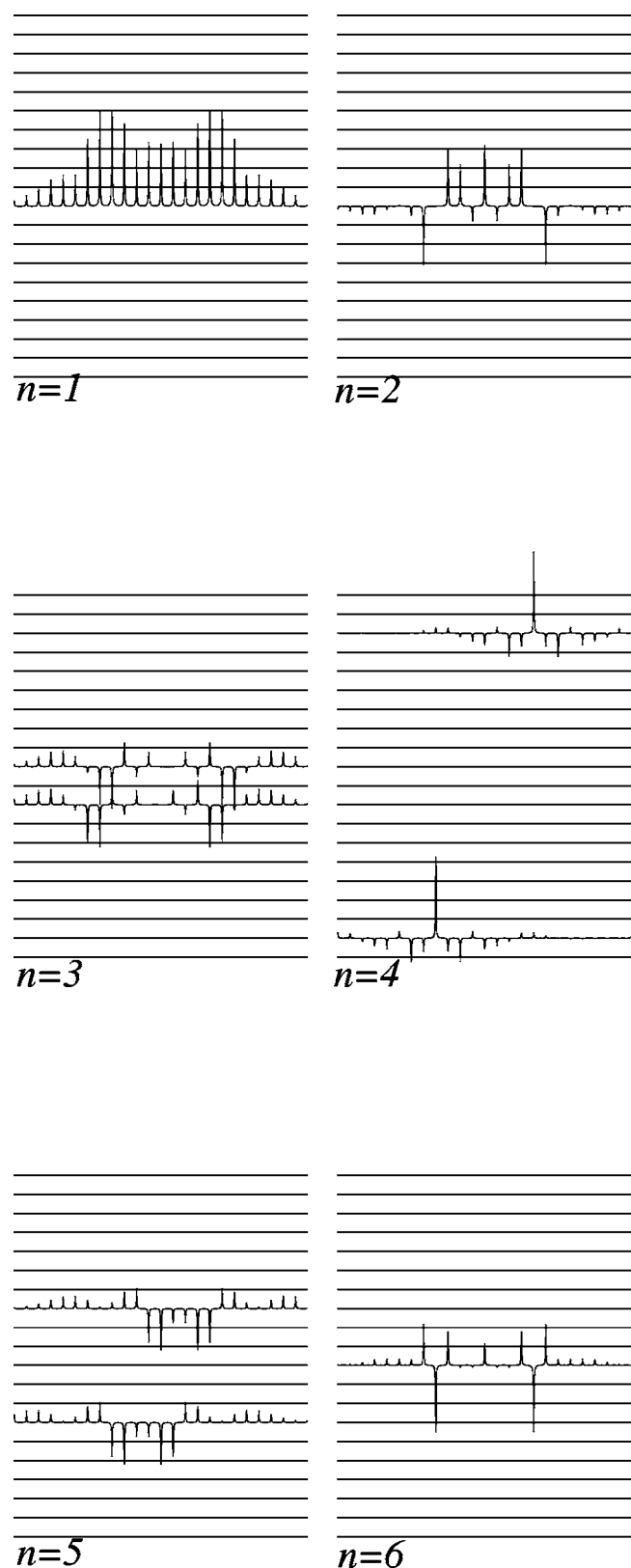


FIG. 3. COF eigenspectra of a rotor-synchronized MAS experiment, calculated numerically for a ratio of the quadrupolar coupling constant to the rotor speed of $C_Q/\nu_r=15.6$.

spectrum allows the reconstruction of the orientational distribution function $P(\beta, \gamma)$, where the probability to find a particular molecular segment at orientation (β, γ) is given by $P(\beta, \gamma) \sin \beta d\beta d\gamma$.

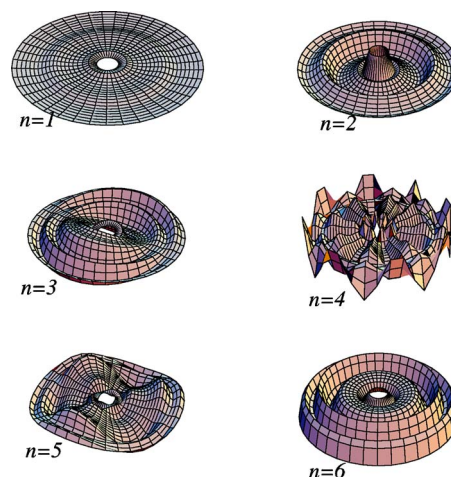


FIG. 4. (Color online) Eigenfunctions $\phi_n(\beta, \gamma)$ of the rotor-synchronized MAS experiment with $C_Q/\nu_r=15.6$. The functions are shown in a stereographic projection, with the angle β varying from 0 to $\pi/2$ from the center to the outside of the graphs. The center point corresponds to the rotor axis direction.

Obtaining $P(\beta, \gamma)$ from a measured spectrum $I_{M,N}$ poses an inverse problem which can be treated within the framework of the conjugate orthogonal function method.¹⁴ In this approach, two sets of orthogonal functions are obtained from an eigenvalue analysis of the correlation matrix $G(\Gamma, \Gamma')$ between spectra corresponding to different orientations $\Gamma=(\beta, \gamma)$ and $\Gamma'=(\beta', \gamma')$. This leads to “eigenspectra” of the method, which in the present case are manifolds of sideband intensities; some examples are shown in Fig. 3. The contributions to the orientational distribution function corresponding to the spectra in Fig. 3 are shown in Fig. 4. As is typical for the conjugate orthogonal function (COF) method, the first eigenfunction, corresponding to the largest eigenvalue, is positive everywhere, with little variation over the orientational domain, whereas the higher eigenfunctions become gradually more oscillatory. It should be noted that eigenfunctions that only show variation in the radial direction (the angle between the CD bond and the rotor axis) correspond to eigenspectra that only have intensity in sidebands $I_{M,N}$ with $M=0$. This is to be expected, since orientational distributions that are symmetric with respect to the rotor axis do not lead to a modulation of the signal with the beginning rotor phase ψ .

In the COF framework, the orientational distribution function is represented as a sum over the COF eigenfunctions $\phi(\beta, \gamma)$

$$P(\beta, \gamma) = \sum_{n=0}^{\infty} p_n \phi_n(\beta, \gamma), \quad (13)$$

where the expansion coefficients p_n are obtained from the measured sideband intensities $I_{M,N}$ by projection onto the COF eigenspectra $\zeta_{M,N}^n$,

$$p_n = \frac{1}{\lambda_{n, M, N=-N_{\max}}} \sum_{M, N=-N_{\max}}^{N_{\max}} I_{M,N} \zeta_{M,N}^n, \quad (14)$$

where λ_n is the n th COF eigenvalue. Note that the eigenfunctions are normalized such that

$$\int_0^\pi \sin \beta d\beta \int_0^{2\pi} d\gamma \phi_n(\beta, \gamma) \phi_m(\beta, \gamma) = \delta_{m,n}, \quad (15)$$

and

$$\sum_{M,N=-N_{\max}}^{N_{\max}} \xi_{M,N}^n \xi_{M,N}^m = \delta_{m,n} \lambda_n. \quad (16)$$

The coefficients p_n can be determined from the experimental data to a precision of

$$(\Delta p_n)^2 = \frac{\xi^2}{\lambda_n}, \quad (17)$$

where ξ^2 is a measure of the noise present in the experimental spectra. In the present case, ξ^2 was obtained from the sum of the squared deviation χ_{\min}^2 between the theoretical isotropic sideband intensities and those measured from a sample known to be isotropic as¹⁵

$$\xi^2 = \left(1 + \frac{p}{n-p} F_{(p,n-p)}^{(0.9)} \right) \chi_{\min}^2, \quad (18)$$

where p is the number of eigenfunctions to be used in the fit, n is the number of relevant sidebands (of order N_{\max}^2), and $F_{(p,n-p)}^{(0.9)}$ is the 0.9 quantile of the F distribution with p degrees of freedom and $n-p$ independently measured data points.

In addition to the direct COF analysis described above, it is also possible to decompose the orientational distribution function into an orthonormal set of Wigner matrix elements as basis functions. This is useful, since it is customary to characterize orientational order by the moments of the orientational distribution function $\langle D_{m,m'}^j(\alpha, \beta, \gamma) \rangle$. In the present case, since we are dealing with zero asymmetry of the EFG tensor, the first Euler angle is irrelevant, and only the moments $\langle D_{0,m'}^j \rangle$ need be taken into account. The Wigner matrix element functions may be used as orthogonal basis functions in the orientational domain much like the COF eigenfunctions introduced above. Unlike the $\phi_n(\beta, \gamma)$, however, the spectra associated with the Wigner matrix elements are not orthogonal. However, examination of the correlation matrix $G_{j m, j' m'}$, obtained from the sideband patterns associated with the Wigner matrix elements, reveals that they come quite close to being orthogonal. Due to the direct dependence of the sideband intensities in (5) on the second polar angle γ , we have $G_{j m, j' m'} = 0$ for $|m| \neq |m'|$. Wigner matrix elements with different major quantum numbers j only overlap if both m and m' are zero. Similarly to the COF eigenfunctions, Wigner matrix elements with $m' = 0$ lead to sideband intensities that vanish for $M \neq 0$, since orientational order that is cylindrically symmetric around the rotor axis is only reflected in a distortion of the relative sideband intensities, and does not lead to a modulation of the sidebands with the rotor phase.

III. EXPERIMENT

The perdeuterated polyethylene (d-PE) was purchased from Polymer Source. The molecular weight of the sample was 133 000 and the polydispersity index was 1.06. This

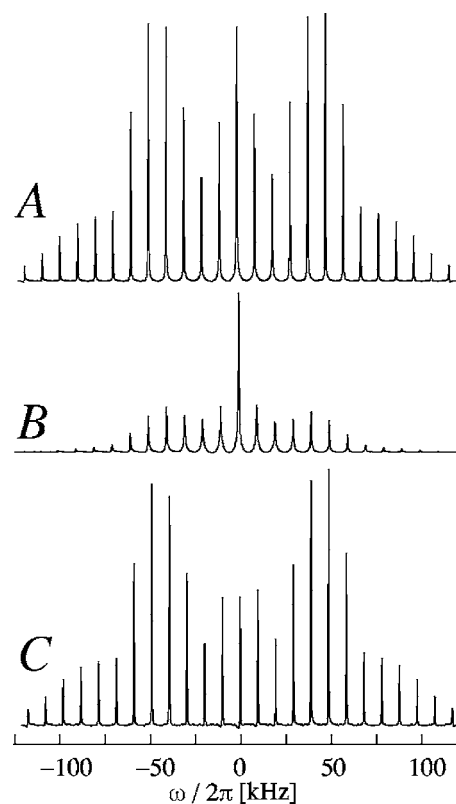


FIG. 5. Deuterium MAS spectra of undeformed, perdeuterated poly(ethylene). (A) Full spectrum; (B) amorphous part selected by presaturation; (C) difference spectrum.

sample was used as received for obtaining the undeformed spectra. The sample used for deformation was prepared by forming a thin film of d-PE by using a heated plate press (at 100 °C). A thin strip ($3 \times 6 \text{ mm}^2$) of this film was subjected to unidirectional cold drawing to 100% deformation. This deformed sample was packed in a 4 mm zirconia rotor with the drawing axis perpendicular to the rotor axis.

NMR experiments were carried out on a Bruker DMX 300 solid-state spectrometer. The DMX 300 spectrometer operates at a field strength of 7.05 T leading to a ^2D Larmor frequency of 46 MHz. All spectra were obtained under 10 kHz MAS speed, with the receiver dead time set to one full rotor period in order to avoid coil ringdown distortions. The pulse sequence used for obtaining the full spectra is shown in Fig. 2. Selective spectra of the amorphous phase were obtained by presaturation of the crystalline phase using a series of 12 $\pi/2$ pulses separated by 50 μs followed by a 50 ms delay. Spectra of the crystalline phase were obtained by subtraction.

IV. RESULTS AND DISCUSSION

The one-dimensional MAS spectrum of undeformed, perdeuterated poly(ethylene) is shown in Fig. 5(A). As is well known, poly(ethylene) is a semicrystalline polymer, and the crystalline and amorphous phases can be distinguished on the basis of their strongly different spin-lattice relaxation times.⁸ Figure 5(B) shows the spectrum of the amorphous part, obtained by preceding the acquisition $\pi/2$ pulse with a train of saturation pulses and a relaxation delay of 50 ms.

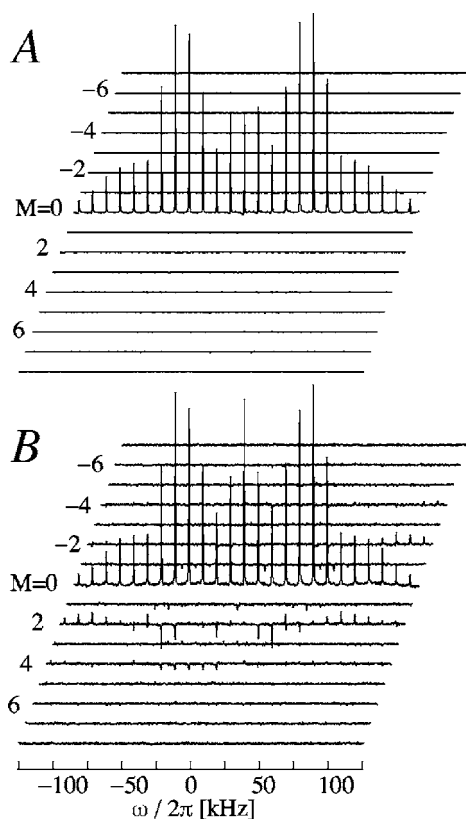


FIG. 6. Deuterium rotor-synchronized MAS spectra of perdeuterated poly(ethylene). The amorphous part has been subtracted from the spectra. (A) Before deformation; (B) after unidirectional cold drawing by 100%.

Since the T_1 relaxation time of the crystalline part is about 2 s at room temperature, this effectively suppresses the signal from PE crystallites. The enhanced mobility of the amorphous regions is reflected in the narrower sideband pattern. In addition, the individual peaks are broader than those in Fig. 5(A).

Subtraction of the amorphous spectrum leads to the spectrum in Fig. 5(C). Note that the broad feet of the peaks (in Fig. 5(A) are fully accounted for by the amorphous part. The crystalline spectrum in Fig. 5(C) is characterized by very narrow lines. Another prominent difference between the full and the crystalline spectrum is the absence of the enhanced centerband.

Figure 6 shows the two-dimensional r-sync MAS spectrum for the crystalline part of both an undeformed and a deformed (cold drawn) sample of poly(ethylene). It has been shown that at high strains, it is the chains and not the lamellar crystallites that orient parallel to the draw direction in the crystalline part of the sample.¹¹ The absence of any intensity in the indirect dimension of Fig. 6(A) shows that the sample is fully isotropic. The two-dimensional (2D) spectrum of the cold-drawn sample is shown in Fig. 6(B). With respect to Fig. 6(A), there is a noticeable change in the intensities along the centerband ($M=0$), and there is substantial intensity in the indirect dimension ($M \neq 0$).

The orientational distribution of C-D bond vectors can be obtained quantitatively from the r-sync MAS spectra by projection onto the COF eigenspectra. The data shown in Fig. 6 have been obtained at a magic-angle spinning speed of

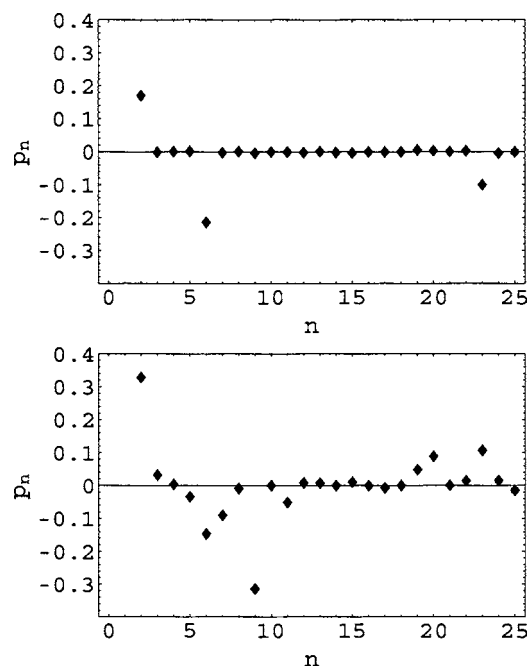


FIG. 7. COF expansion coefficients obtained from top: Undeformed poly(ethylene); bottom: cold-drawn poly(ethylene). The experimental stochastic errors are smaller than the symbol size.

$\nu_r = 10$ kHz. COF eigenspectra and eigenfunctions have been computed numerically for this value; the first six of them (corresponding to the six largest eigenvalues) are shown in Figs. 3 and 4, respectively. It should be noted that the first eigenfunction $n=1$ is almost constant. Therefore, the first eigenspectrum closely resembles the spectrum obtained from an isotropic sample. It is interesting to note that each eigenspectrum exhibits nonzero intensity only for a specific value of $|M|$. This is a consequence of the direct dependence of the sideband phases on the second Euler angle γ . Indeed, eigenspectra with intensity only in the centerband ($M=0$) correspond to eigenfunctions that are rotationally symmetric with respect to the rotor axis. This is evident in Figs. 3 and 4 for $n=1, 2$, and 6.

The resulting expansion coefficients are plotted in Fig. 7. It should be noted that $p_1=1$ by normalization. For the isotropic sample (top panel in Fig. 7), most expansion coefficients are zero within experimental precision. The only exceptions are p_2 , p_6 , and p_{23} . Inspection of the corresponding eigenfunctions reveals that they are rotationally symmetric with respect to the rotor axis. This means that they depend exclusively on the polar angle β . As a consequence, the corresponding eigenspectra contain intensity only in the centerband (I_{0N}). In the case of the isotropic sample, the nonzero coefficients reflect the experimental distortion of the observed sideband intensities from the theoretical pattern expected for the given value of $C_Q/\nu_r=15.6$. Several sources can be considered for such deviations. On the one hand, residual mobility, even in the crystalline parts of the sample, may lead to slight alterations of the sideband intensities. In addition, the excitation profile of the pulse sequence may not be perfectly uniform, and the bandwidth of the MAS probe used for the experiment is limited, leading to an enhancement of the center of the spectrum at the expense of the periphery.

TABLE I. Moments of the orientational distribution determined from r-sync MAS ^2D NMR.

	PE deformed
$\langle D_{00}^0 \rangle$	1.000 ± 0.014
$\langle D_{00}^2 \rangle$	0.050 ± 0.033
$\langle D_{01}^2 \rangle = -\langle D_{0-1}^2 \rangle$	-0.020 ± 0.019
$\langle D_{02}^2 \rangle = \langle D_{0-2}^2 \rangle$	0.138 ± 0.020
$\langle D_{00}^4 \rangle$	0.084 ± 0.001
$\langle D_{01}^4 \rangle = -\langle D_{0-1}^4 \rangle$	-0.007 ± 0.010
$\langle D_{02}^4 \rangle = \langle D_{0-2}^4 \rangle$	0.024 ± 0.008
$\langle D_{03}^4 \rangle = -\langle D_{0-3}^4 \rangle$	-0.009 ± 0.009
$\langle D_{04}^4 \rangle = \langle D_{0-4}^4 \rangle$	0.012 ± 0.005

In principle, it would be possible to either account for these imperfections theoretically, or compensate some of them experimentally. However, the linearity of the COF approach allows for a much simpler solution. Since it is only the *deviation* from an isotropic orientational distribution function that is of interest, it is sufficient to subtract the expansion coefficients obtained from a sample that is known to be isotropic. This approach has been adopted in the present contribution.

Even though the expansion coefficients shown in Fig. 7 contain all the orientational information that can be extracted from the experimental spectra, they do not present it in an intuitively meaningful form. Using a unitary transformation, it is possible to recast this information into moments of the orientational distribution function based on Wigner matrix elements $\langle D_{mn}^l(\alpha, \beta, \gamma) \rangle$.¹⁶ In the present case, only moments with $m=0$ are relevant due to the axial symmetry of the ^2D quadrupolar tensor. Moments with $l=2,4$ obtained for the above case of cold-drawn poly(ethylene) are given in Table I. The orientational order induced by the cold-drawing process is reflected mainly in $\langle D_{02}^2 \rangle$, with all other moments close to zero within experimental uncertainty.

The orientational distribution function is represented as a pole figure in stereographic projection in Fig. 8. The contour where $P(\beta, \gamma)=1$, separating areas of enrichment from areas of depletion, is indicated as a bold black line. The origin of the graph corresponds to the rotor axis (R), which is in the plane of the PE film, perpendicular to the cold-drawing direction is indicated as D .

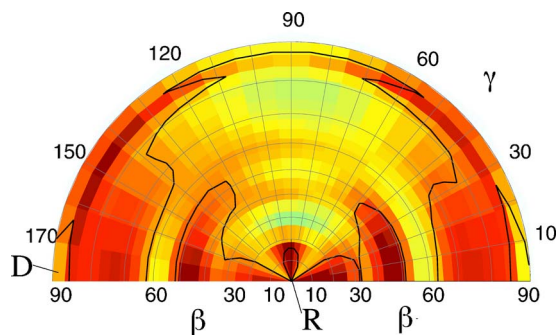


FIG. 8. (Color online) Orientational distribution of cold-drawn d-PE in stereographic projection. Bright areas are depleted, and dark areas are enriched. The neutral line [$P(\beta, \gamma)=1$] is indicated in solid black. The origin of the graph corresponds to the rotor direction (R). The cold-drawing direction is indicated as D . The normal of the PE film corresponds to $(\beta, \gamma) = (90^\circ, 90^\circ)$.

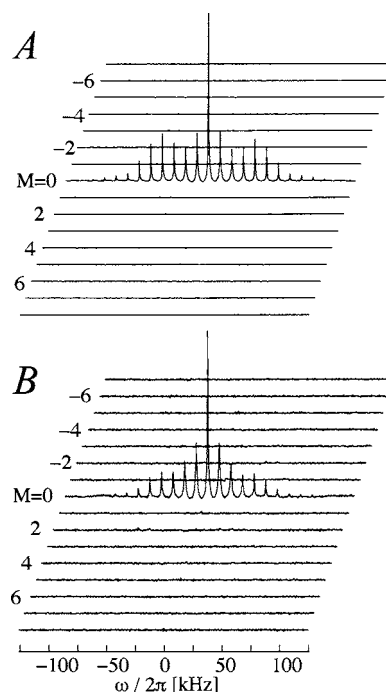


FIG. 9. Deuterium rotor-synchronized MAS spectra of perdeuterated poly(ethylene). The amorphous part has been selected by presaturation. (A) Before deformation; (B) after unidirectional cold drawing by 100%.

rection. The point $(\beta, \gamma) = (90^\circ, 90^\circ)$ corresponds to the normal to the PE film, whereas the cold-drawing direction is indicated as D in the plot.

It is clearly visible in Fig. 8 that the C–D bond axis is enriched along the draw direction, at the expense of the film thickness direction. This is in agreement with the well-known fact that cold drawing of semicrystalline PE leads to orientation of the chain segments parallel to the draw direction which in turn leads the crystal lamellae to be stacked perpendicular to the draw axis.⁸

The part of the r-sync MAS spectrum related to the amorphous component of PE is shown in Fig. 9. As discussed above, the sideband intensity distribution is different from the crystalline case due to the increased segmental mobility. Unfortunately, it is impossible to extract quantitative orientational data for the amorphous part in the absence of a detailed model for the thermal segmental reorientation. However, some qualitative observations are possible. Unlike the crystalline part, the amorphous part exhibits no intensity in the indirect dimension for $M \neq 0$ after deformation. This means that the orientational distribution of the amorphous segments is at least symmetric with respect to the rotor axis. In contrast to the sideband spectra ($M \neq 0$), the centerband spectrum ($M=0$) does show clear differences before and after deformations. On the one hand, this could be caused by orientational order (nonuniform distribution of Euler angles β). Another possible cause, however, is a change in the molecular dynamics induced by the deformation. In order to distinguish between these two alternatives, the sample was loaded into the rotor in a different orientation, with the drawing direction parallel instead of perpendicular to the rotor axis. The resulting spectrum (not shown) was indistinguishable from the one shown in Fig. 9(B). We therefore tenta-

tively conclude that the cold-drawing process has affected the molecular dynamics of the amorphous phase, but did not lead to noticeable segmental orientation.

V. CONCLUSIONS

The quadrupolar rotor-synchronized MAS experiment has been successfully applied to quantify orientational order in cold-drawn semicrystalline poly(ethylene). This could not have been achieved using the standard r-sync MAS experiment due to the smallness of ^{13}C chemical shielding anisotropy in PE. The experimental r-sync MAS spectra can be conveniently processed using the conjugate orthogonal function approach, and can then be expressed either as a orientational distribution function $P(\beta, \gamma)$, or in terms of the Wigner moments. Due to the negligible asymmetry of the electric-field gradient tensor in C-D bonds, two Euler angles are sufficient to describe its orientation. This can be seen as an advantage, since it simplifies the data analysis considerably. On the other hand, only a directional distribution (pole figure) is obtained, instead of a full orientational distribution function of the molecular segments containing the deuterium labels.

In agreement with earlier measurements, cold drawing of PE has been found to induce substantial orientational ordering of the crystalline domains. By contrast, the amorphous part of PE does not seem to develop preferential orientation at the level of cold drawing (100%) investigated. However, changes in the sideband intensity distribution suggest that the

rate and/or the geometry of the segmental reorientation dynamics in the amorphous phase of PE are affected by cold drawing.

ACKNOWLEDGMENT

The support of the National Science Foundation in the form of a CAREER grant to one of the authors (M.U.) (DMR 0094290) is gratefully acknowledged.

- ¹V. J. McBrierty, J. Chem. Phys. **61**, 872 (1974).
- ²R. Hentschel, J. Schlitter, H. Sillescu, and H. Spiess, J. Chem. Phys. **68**, 56 (1978).
- ³R. Hentschel, H. Sillescu, and H. W. Spiess, Polymer **22**, 1516 (1981).
- ⁴G. S. Harbison and H. W. Spiess, Chem. Phys. Lett. **124**, 128 (1986).
- ⁵G. S. Harbison, V.-D. Vogt, and H. W. Spiess, J. Chem. Phys. **86**, 1206 (1987).
- ⁶P. M. Henrichs, Macromolecules **20**, 2099 (1987).
- ⁷B. F. Chmelka, K. Schmidt-Rohr, and H. W. Spiess, Macromolecules **26**, 2282 (1993).
- ⁸K. Schmidt-Rohr and H. W. Spiess, *Multidimensional Solid-State NMR and Polymers* (Academic, San Diego, 1994).
- ⁹M. Utz, M. Tomaselli, R. R. Ernst, and U. W. Suter, Macromolecules **29**, 2909 (1996).
- ¹⁰M. Utz, A. S. Atallah, P. Robyr, U. W. Suter, and R. R. Ernst, Macromolecules **32**, 6191 (1999).
- ¹¹K. Schmidt-Rohr, M. Hehn, D. Schaefer, and H. W. Spiess, J. Chem. Phys. **97**, 2247 (1992).
- ¹²M. Utz, J. Eisenegger, U. W. Suter, and R. R. Ernst, J. Magn. Reson. **128**, 217 (1997).
- ¹³J. Herzfeld and A. E. Berger, J. Chem. Phys. **73**, 6021 (1980).
- ¹⁴M. Utz, J. Chem. Phys. **109**, 6110 (1998).
- ¹⁵N. R. Draper and H. Smith, *Applied Regression Analysis* (Wiley, New York, 1981).
- ¹⁶M. Utz, Ph.D. thesis No. 12717, Eidgenössische Technische Hochschule (ETH), Zurich, 1998.